

Cite this: *Soft Matter*, 2011, **7**, 10395

www.rsc.org/softmatter

PAPER

# Lubrication in soft rough contacts: A novel homogenized approach.

## Part I - Theory

Michele Scaraggi,<sup>\*ab</sup> Giuseppe Carbone,<sup>a</sup> Bo N. J. Persson<sup>c</sup> and Daniele Dini<sup>b</sup>

Received 25th January 2011, Accepted 20th July 2011

DOI: 10.1039/c1sm05128h

We study the lubricated steady sliding contact between rough surfaces of (elastically) soft solids. A novel mean field theory of mixed lubrication is presented, which takes into account the coupled effect of asperity–asperity and asperity–fluid interactions. We calculate the fluid flow factors, and discuss the nature of the transition from the boundary lubrication regime, where the normal load is supported by the asperity–asperity interactions (sometimes mediated by boundary films), to the hydrodynamic regime, where a thin fluid film prevents direct contact between the mating surfaces.

### I. Introduction

The investigation of the role of roughness in contact mechanics has attracted the attention of a large number of scientists in the last two centuries.<sup>1–4</sup> As a result, it is now well known that the presence of roughness between contacting interfaces usually results in an incomplete contact,<sup>5–7</sup> the global or local characteristics of which are of extreme importance in many practical problems. Indeed, macroscopic contact properties such as friction, electrical (and thermal) contact resistance, wear and adhesion are fundamentally related to the surface roughness characteristics.<sup>8</sup> In the last decade this concept has been widely confirmed and replicated by bio-mimetics researchers, who have experimentally observed that a correctly designed hierarchical surface structuring allows one to efficiently obtain tailored tribological/surface properties. The case of the geckos adhesive-like surfaces research is an example of this. Indeed, geckos (*Gekko gekko*) and many insects show an extraordinary climbing ability on vertical surfaces and ceilings, and this biological mechanism of attachment is ascribed to the synergy of roughness hierarchy, fluid secretion (capillarity and viscosity effects) and van der Waals interaction.<sup>9,10</sup>

Tailoring surface properties by surface micro (nano-) structures fabrication is actually state of art,<sup>11</sup> and involves a wide range of applications, from life science (*e.g.* cell adhesion/proliferation, tissue engineering, tactile perception) to biology (*e.g.* tailored adhesion, self cleaning) and engineering (*e.g.* microfluidics, sealants, surface structuring for manufacturing tools and bearings). However, despite the large amount of research effort in the surface functionalization, the understanding of the fundamental phenomena occurring at the contact

between interfaces is still far from being fully achieved.<sup>12</sup> One of the reasons for such a lack of knowledge is due to the very large number of degrees of freedom introduced by the surface roughness description in the contact problem formulation. Indeed, the roughness of real (Nature- or man-made) surfaces can span length scales from a few millimetres to atomic dimensions, resulting in surface fluctuations occurring in a  $\sim 6$  orders wavelengths range. Then, it is not surprising that the first appearance of theoretical investigations were on a statistical basis, and this has been the case of the rough dry contact mechanics of elastic bodies;<sup>6</sup> in the soft matter field, actually a large amount of fundamental theoretical research on rough dry contact mechanics and bio-mimetics has been performed by Persson<sup>13</sup> and co-workers.

In the case of the lubricated contact of rough bodies, which are the focus of this paper, theoretical investigations appeared much later than Ref. 6, and essentially in the form of numerical calculations on deterministic models.<sup>14,15</sup> This should not be a surprise since the most commonly used (and maybe simplest) mathematical description of fluid lubrication, namely the Reynolds equation, does not generally allow analytical treatments, even when it is applied to very simple geometrical configurations. Actually, research on the lubricated contact of rough bodies is focused on particular aspects of the problem itself. As an example in the static case, the hydraulic conductivity of a contact interface, which is of utmost importance for industrial applications (*e.g.* sealants, tires) as well as for life science (dewetting at soft rough interfaces), has been recently modeled in the case of isotropic surfaces recurring to percolation theory arguments,<sup>16–18</sup> which are in good agreement with experiments.<sup>19</sup> Experimental observations of sliding contacts made with optical interferometry (see *e.g.* Ref. 20) have instead confirmed the existence of the so called *viscous flattening*, an asperity flattening induced by fluid viscous actions at the asperity scale, which results in an effective smoothing of the sliding surfaces. This phenomenon has also been predicted by numerical calculations of wavy surfaces.<sup>21</sup> Interestingly, it has been found

<sup>a</sup>DIMeG, Politecnico di Bari, V.le Japigia 182, 70126 Bari, Italy

<sup>b</sup>Department of Mechanical Engineering, Imperial College London, South Kensington Campus, Exhibition Road, SW7 2AZ London, UK

<sup>c</sup>IFF, FZ-Jülich, 52425 Jülich, Germany

that the contribution of different roughness length scales on the fluid film and fluid pressure are effectively uncoupled in the Fourier space, so that the viscous flattening, which admits a general formulation in wavevector space,<sup>22–24</sup> can be separately calculated for each wavelength. Moreover, it has been shown that the amplitude of the long wavelengths roughness is reduced considerably inside the contact, whereas short wavelengths roughness is only barely affected by the fluid action;<sup>22</sup> this is also in agreement with the existing experimental evidence.<sup>20</sup>

On a different side, friction measurements have been carried out for the sliding contact of soft isotropically rough surfaces at different degrees of hydrophobicity/hydrophilicity and for different values of rms (root-mean-square) roughness.<sup>25</sup> In particular, in Ref. 25 the authors showed that very different Stribeck† curves can be obtained in the boundary‡ and mixed§ lubrication regimes by adopting rough surfaces with different rms. Moreover, they also observed that changing the surface energy of the contact pair allows the further manipulation of the friction curves, *e.g.* the boundary lubrication regime could not be formed for a hydrophilic contact. A theoretical explanation of such friction experiments has been recently proposed in Ref. 12.

In Ref. 26, instead, some of us have performed friction measurements in the case of a smooth steel rotating ball in lubricated contact with a fixed rough PDMS surface; moreover, the rubber sample was characterized by a strongly anisotropic roughness. We showed that the roughness anisotropy has a large influence on the shape of the friction–velocity curve as a consequence of the occurrence of local (asperity scaled) hydrodynamic lubrication conditions at the contact interface. These micro-bearings conditions were experienced for the transverse roughness orientation (*i.e.* for the roughness main grooves aligned perpendicularly with the sliding direction), but were not observed for the longitudinal orientation (simply obtained rotating the transverse roughness sample by 90°). In particular, the transverse roughness lubrication was characterized by a secondary hydrodynamic friction stage located in a velocity range which does not overlap with the primary (or macroscopic) hydrodynamic friction stage (*i.e.* the friction range due to the macroscopic ball shape). All the cited experimental results suggest the presence of a strong link between surface roughness, viscous flattening and friction in soft contacts. However, they also highlight the lack of fundamental theoretical research on the lubricated contact of rough bodies, since, to the best of the author's knowledge, there exists no comprehensive theory able to capture and describe, at least qualitatively, such phenomena within a unique framework.

The first general insight into the lubrication of rough surfaces dates back to the late seventies, when Patir and Cheng (P&C) carried out the first numerical calculations,<sup>27,28</sup> and Sun presented a thorough theoretical investigation.<sup>29</sup> P&C<sup>27,28</sup> recognised the possibility to calculate the average fluid dynamics occurring at the interface of mixed lubricated contacts by solving effective fluid equations involving a set of functions (depending on the nature of the surface roughness), usually denoted as flow

factors. These flow factors were determined by solving the fluid flow equation for small interfacial rectangular regions containing the rough surfaces, and averaging over several realisations of the rough surfaces. The basic assumption in this approach is the wide separation of length scales, *i.e.* one assumes that the surface roughness occurs at length scales much shorter than the macroscopic contact size of the solid objects. In this case the flow factors completely describe the influence of the surface roughness on the (average) fluid flow observed at the macroscopic scale.

After the P&C model, a number of interesting studies have been performed to model mixed lubricated contacts, see *e.g.* Refs. 30–34. In these models the local elastic deformation (at the asperities scale), resulting from the asperity–asperity and asperity–fluid interactions, was not included. However, as recently shown by Meng and co-workers,<sup>35</sup> this approximation may result in non-negligible errors when the average interfacial separation  $\bar{u}$  approaches the surface rms roughness  $h_{\text{rms}}$ , a condition typically encountered in mixed lubrication. Indeed, as  $\bar{u}$  decreases the amount of direct asperity–asperity contact will increase, influencing the number and the size of non-contact domains that can be filled by the lubricant. As we show below, by increasing the load, the contact patches start to merge into larger multi-connected domains, which behave as closed labyrinths, thus inhibiting the fluid flow. This occurs at values of the normalized area of solid contact sufficiently close to the percolation threshold, see *e.g.* the recent studies on percolation threshold in static seals.<sup>16–18</sup> At the percolation threshold, or at larger contact areas, a portion of the non-contact surface area may be filled by the lubricant. However, the fluid remains entrapped by the solid walls formed by the contacting asperities, and cannot flow out, therefore providing no contribution to the total (average) flow at the interface. This effect is likely to be extremely important in mixed lubrication since the repulsive hydrostatic force at the interface depends on the fluid filled areas, and to the best of our knowledge there is no thorough investigation of this phenomenon in the scientific literature.

In this work, which has been inspired by the novel experimental results of Ref. 26, we propose a second order expansion lubrication theory. We investigate the role of random roughness on the average flow and friction of soft (compliant) lubricated contacts, such as those occurring in a wide range of applications, from the classical tire–road (or seal–shaft) contact, to the soft contacts in bio-tribological applications. In our theory the asperity–asperity and asperity–fluid interactions are coupled in a consistent formulation of the contact mechanics occurring at the interface. Using this model we discuss the transition (observed at the macro-scale) from the boundary lubrication to the hydrodynamic lubrication regime as a consequence of averaging different lubrication states occurring at different locations at the interface. We also confirm some general findings by Hooke and Venner<sup>21</sup> related to the asperity flattening.

The paper is outlined as follows. The lubrication theory is presented in Secs. II to V. In Sec. II we summarize the mean field theory for the asperity–asperity interactions, which is based on the Persson's multiscale contact mechanics.<sup>7</sup> In Secs. III to V we characterize the average fluid flow at the interface in terms of flow factors, and we derive the average lubrication equation by enforcing mass conservation to the average fluid flow. Numerical results and general considerations are presented in the companion paper (Ref. 36).

† Friction as function of the product between viscosity and sliding velocity.

‡ Lubrication regime where the contact normal load is supported mainly by asperity–asperity interactions.

§ Lubrication regime where the contact normal load is supported by both asperity–asperity and fluid–asperity interactions.

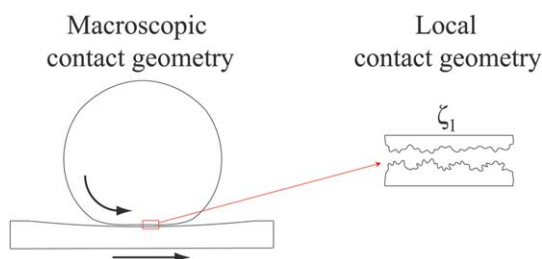
## II. The homogenized asperity–asperity interactions

We consider the *macroscopically steady sliding* motion of an elastic ball (or cylinder) pressed against an elastic substrate. We also assume that both the ball and the substrate are covered with random roughness. The notation *macroscopically steady sliding* simply means that, although at the macro-scale the system appears in a condition of steady-state, at the micro-scale the presence of roughness on both surfaces determines local (at the asperity-scale) transient motions (local squeeze effects), which are averaged out and cannot be observed at the macroscopic scale, *i.e.* at the length scale of the Hertzian contact. Fig. 1 illustrates the essential features of the model: we assume that the macroscopic contact size is much larger than the largest roughness length scale. This wide difference of length scales enables averaging over the roughness fluctuations, thus obtaining effective equations for smooth surfaces which are much more suitable for implementation from a computational point of view.

Due to the generally low pressures (of order MPa) occurring in soft contacts, the lubricant can be assumed to be Newtonian, *i.e.* with shear-rate independent and pressure independent viscosity and density. We also neglect thermal effects, as well as the occurrence of asperity-scale cavitation, the latter being actually under investigation by some of the authors. In some cases a dewetting transition plays a fundamental role in determining the boundary friction value<sup>25</sup> (see also Ref. 37 for a review on the topic) and the region occupied by the fluid. However, this phenomenon is only partially modeled in the methodology proposed here by properly choosing the boundary shear stress. Moreover, we assume that the sliding surfaces are characterised by random roughness with known statistical properties (*e.g.* the power spectral density (PSD)<sup>38</sup>).

In this section we present a mean field theory where the asperity–asperity interactions at the interface are described using Persson's contact mechanics formulation.<sup>7,39</sup> Each quantity discussed below must be interpreted as an ensemble average.

For adhesionless elastic contacts, the (average) normalized real area of solid contact can be calculated as  $A(\zeta_1)/A_0$  (where  $A_0$  is the nominal contact area), where  $q_1 = q_0\zeta_1$  corresponds to the largest roughness frequency and



**Fig. 1** The geometry of two solids in sliding contact with a fluid in between, observed at the macroscopic scale (left) and at the largest magnifications  $\zeta_1$  in the contact area (right). For randomly rough surfaces, the smallest asperity length scale  $\lambda_1 = L/\zeta_1$  can be many orders of magnitude smaller than the macroscopic contact size  $L$ . In this case a deterministic approach to the contact problem would require a very large computational effort, and an analytical (average field) theory should be preferred for a fast estimation of the contact characteristics.

$$\frac{A(\zeta)}{A_0} = \operatorname{erf}\left(\frac{\sqrt{2}\sigma_0}{E^*[\nabla h]_{\text{rms}}(\zeta)}\right), \quad (1)$$

where:

$$[\nabla h]_{\text{rms}}^2(\zeta) = \langle [\nabla h(\mathbf{x})]^2 \rangle = \int_{|\mathbf{q}| < q_0\zeta} d^2q q^2 C(\mathbf{q}),$$

$\zeta = q/q_0$  is the magnification,  $\sigma_0$  is the average (or nominal) solid contact pressure and the combined power spectral density is  $C(\mathbf{q}) = C_1(\mathbf{q}) + C_2(\mathbf{q})$ .<sup>38</sup> The subscripts (1 & 2) refer to the two different surfaces respectively. The PSD of each surface is defined as:

$$C_i(\mathbf{q}) = \frac{1}{(2\pi)^2} \int d^2x \langle h_i(\mathbf{x})h_i(\mathbf{0}) \rangle e^{-i\mathbf{q}\cdot\mathbf{x}},$$

where  $\langle \dots \rangle$  stands for ensemble average, and  $h_i(\mathbf{x})$  is the surface height of the  $i$ -th surface with  $\langle h_i(\mathbf{x}) \rangle = 0$ . Also we have defined:

$$1/E^* = (1 - \nu_1^2)/E_1 + (1 - \nu_2^2)/E_2,$$

where  $E_i$  and  $\nu_i$  are Young's elastic modulus and Poisson's ratio of  $i$ -th solid respectively. In the ideal case of self affine isotropic roughness the PSD has a very simple analytical formulation:  $C(q) = C_0(q/q_0)^{-2(H+1)}$ , where  $C_0 = h_{\text{rms}}^2 H / [\pi q_0^2 (1 - \zeta_1^{-2H})]$ ,  $H$  is the Hurst exponent related to the fractal dimension  $D_f$  through the relation  $H = 3 - D_f$ ,  $q_0$  is the large wavelength roll-off frequency, and  $q_1 = \zeta_1 q_0$  is the small wavelength cut-off frequency of the PSD. Fractal surfaces, or more generally, surfaces where only a fraction of their spectral content is characterized by self-affine properties, are very common, *e.g.* asphalt road surfaces, or fracture surfaces of brittle materials.<sup>13</sup>

In the case of linear viscoelastic solids, or in the case of contact between solids of finite thickness (*e.g.* for thin polymer or rubber coatings), the equations above are slightly modified as reported in Ref. 7 for isotropic roughness, and in Ref. 39 for the general case of anisotropic roughness. In the absence of viscoelastic effects, the average shear stress at the solid–solid contact is assumed to be:

$$\tau^s = \alpha \sigma_f,$$

where  $\sigma_f$  is the frictional shear stress acting in the asperity–asperity contacts and  $\alpha = A(\zeta_1)/A_0$  is the relative contact area. The shear stress in the contact regions,  $\tau^s$ , is aligned along the resultant sliding direction.

The average interfacial separation in the apparent contact areas at the magnification  $\zeta$  can be calculated from Refs. 40 and 41 as:

$$\bar{u}(\sigma_0, \zeta) = \sqrt{\pi} \int_{\zeta q_0}^{q_1} dq q^2 C^{\text{avg}}(q) w(\zeta, q) \int_{A_0 \sigma_0 / A(\zeta)}^{\infty} dp' \frac{e^{-[w(\zeta, q)p' / E^*]^2}}{p'}, \quad (2)$$

where  $C^{\text{avg}}(q) = C_1^{\text{avg}}(q) + C_2^{\text{avg}}(q)$ ,  $C_i^{\text{avg}}(q) = (2\pi)^{-1} \int d\phi C_i(\mathbf{q})$ ,<sup>39</sup> and where:

$$\omega(\zeta, q) = \left( \pi \int_{\zeta q_0}^q dq' q'^3 C^{\text{avg}}(q') \right)^{-1/2}. \quad (3)$$

In order to simplify the notation, in the remaining part of the article the macroscopic (locally averaged) interfacial separation  $\bar{u}(\sigma_0, 1)$  will be simply denoted by  $\bar{u}$ .

When the magnification increases from  $\zeta$  to  $\zeta + \Delta\zeta$  a portion,  $A(\zeta) - A(\zeta + \Delta\zeta)$ , of the surface area moves out of the contact, and is characterized by a *local* average interfacial separation  $u_1(\zeta)$ , see Fig. 2. The latter quantity is related to Eqns. (1) and (2) through the following equality:

$$\bar{u}(\zeta)A(\zeta) = - \int_{\zeta}^{\zeta_1} dz A'(z) u_1(z) \quad (4)$$

which can be differentiated in  $\zeta$  to give  $u_1(\zeta) = [\bar{u}(\zeta)A(\zeta)]'/A'(\zeta)$ .<sup>40,41</sup>

We now determine an approximate relation for the mean square (*ms*) roughness  $\langle h^2 \rangle_{\text{dry}}$ , which represents the amount of height fluctuations occurring at the interfacial voids in dry contacts. It is clear that the more the surfaces are in intimate contact, the less is the average separation (and the total amount of voids at the interface) and, hence, the smaller is  $\langle h^2 \rangle_{\text{dry}}$ . In the case of large separations,  $\langle h^2 \rangle_{\text{dry}} \rightarrow h_{\text{rms}}^2$ , where  $h_{\text{rms}}$  corresponds to the *ms* of the undeformed surface roughness.

Let  $P_n(u)$  be the probability distribution of interfacial separations in the non-contact surface area  $A_n = A_0 - A_c$ , where  $A_c = A(\zeta_1)$  is the area of real contact and  $A_0 = A(1)$  the nominal contact area. We can write:

$$P_n = \frac{1}{A_n} \int_{A_n} d^2x \delta(u - u(\mathbf{x})),$$

where  $u(\mathbf{x})$  is the interfacial separation at point  $\mathbf{x}$  in the non-contact region. Note that:

$$\int du P_n(u) = 1,$$

and

$$\int du u P_n(u) = \frac{1}{A_n} \int_{A_n} d^2x u(\mathbf{x}) = \frac{A_0}{A_n} \bar{u} = u_n$$

is the average surface separation in the non-contact area. We can therefore re-write  $P_n$  in the following form:

$$P_n = \frac{1}{A_n} \int_1^{\zeta_1} d\zeta [-A'(\zeta)] \langle \delta(u - u(\mathbf{x})) \rangle_{\zeta}.$$

Here  $\langle \dots \rangle_{\zeta}$  stands for averaging over the surface area which moves out of contact as the magnification changes from  $\zeta$  to  $\zeta + d\zeta$ . It should be noted that:

$$\langle u(\mathbf{x}) \rangle_{\zeta} = u_1(\zeta),$$

as shown in Fig. 2. Thus, we obtain:

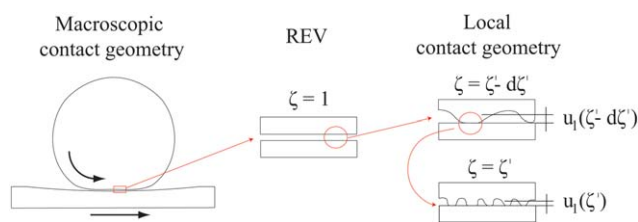
$$\begin{aligned} \langle h^2 \rangle_{\text{dry}} &= \int du P_n(u) (u - u_n)^2 = \frac{1}{A_n} \int d\zeta [-A'(\zeta)] \langle (u(\mathbf{x}) - u_n)^2 \rangle_{\zeta} \\ &= \frac{1}{A_n} \int d\zeta [-A'(\zeta)] \langle ([u(\mathbf{x}) - u_1(\zeta)] + [u_1(\zeta) - u_n])^2 \rangle_{\zeta}. \end{aligned}$$

Expanding the square and exploiting the fact that:

$$\langle [u(\mathbf{x}) - u_1(\zeta)] \rangle_{\zeta} = 0,$$

we get:

$$\langle h^2 \rangle_{\text{dry}} = \frac{1}{A_n} \int d\zeta [-A'(\zeta)] \left[ \langle (u(\mathbf{x}) - u_1(\zeta))^2 \rangle_{\zeta} + (u_1(\zeta) - u_n)^2 \right].$$



**Fig. 2** The geometry of two solids in sliding contact with a fluid in between, observed at a different contact magnification.  $u_1(\zeta')$  represents the average separation in the apparent contact areas which come out of contact when the magnification is increased from  $\zeta' - d\zeta'$  to  $\zeta'$ .

It is clear that the surfaces which move out of contact as the magnification increases from  $\zeta$  to  $\zeta + d\zeta$  will have short-wavelength roughness with wavevectors  $q > \zeta q_0$ . Thus the real separation between these surfaces is not  $u_1(\zeta)$  but fluctuates around this value. One may approximately take this into account by using

$$\langle (u(\mathbf{x}) - u_1(\zeta))^2 \rangle_{\zeta} \approx h_{\text{rms}}^2(\zeta),$$

where  $h_{\text{rms}}^2(\zeta)$  is the *ms* roughness amplitude including only the roughness components with wavevector  $q > q_0\zeta$ . We may approximately write

$$h_{\text{rms}}^2(\zeta) = \int_{q > q_0\zeta} d^2q C(q).$$

Thus we get

$$\langle h^2 \rangle_{\text{dry}} \approx \frac{1}{A_n} \int d\zeta [-A'(\zeta)] \left[ h_{\text{rms}}^2(\zeta) + (u_1(\zeta) - u_n)^2 \right].$$

This expression for  $\langle h^2 \rangle_{\text{dry}}$  involves quantities which are known within the contact mechanics theory of Persson.  $u_n$ , defined as the average interfacial separation in the non contact areas, is in the following identified with the symbol  $u$ . Note that  $u = \bar{u}(1 - \alpha)$ .

Let us define the “smoothing” parameter

$$\varepsilon^s(\bar{u}) = \langle h^2 \rangle_{\text{dry}} / h_{\text{rms}}^2. \quad (5)$$

The parameter  $\varepsilon^s(\bar{u})$  defines the amount of apparent flattening of the initial roughness occurring in the non contact areas due to the asperity–asperity interactions.

### III. The homogenized fluid-flow equations

In this section we determine the average fluid flow at the interface between contacting elastic solids with random roughness. We use the classical Reynolds thin film fluid flow model,<sup>42</sup> and we assume that no (micro-) cavitation occurs at the interface, so that the amount of the load supported by the fluid–asperity interactions is only due to the asymmetrical deformation of the asperities. However, neglecting cavitation is not a real limitation, since it has been shown that for elastically soft solids like rubber,<sup>12</sup> this approximation results only in small errors, so we believe that the main findings of our model must not be qualitatively affected by the non-cavitation assumption.

For Newtonian fluids the general hydrodynamic lubrication equations can be written in a form that can be easily linked to the Reynolds equation:

$$\mathbf{J}(\mathbf{x}, t) = -\frac{s^3}{12\mu}\nabla p + \mathbf{U}_m s$$

$$0 = \frac{\partial s}{\partial t} + \nabla \cdot \mathbf{J}, \quad (6)$$

where  $\mathbf{x}$  is the in-plane position vector,  $\mathbf{J}(\mathbf{x}, t)$  is the fluid flow vector,  $s$  is the local thickness of the fluid film,  $\mathbf{U}_m = (\mathbf{U}_1 + \mathbf{U}_2)/2$  is the mean surfaces velocity (where  $\mathbf{U}_i$  is the velocity of the  $i$ -th surface) and  $p = p(\mathbf{x}, t)$  is the fluid pressure at the interface. Since at the interface some asperities are in direct solid–solid contact, the domain  $\Omega$  where fluid is expected to be present is in general a multi-connected region, whose boundaries,  $\partial\Omega$ , of which correspond to the solid walls formed by the direct solid–solid asperity contacts. At these boundaries the fluid flow vector  $\mathbf{J}$  must satisfy the condition  $\mathbf{J} \cdot \mathbf{n} = 0$ , where  $\mathbf{n}$  is the unit vector normal to the boundary. Observe that the walls of the asperities in solid–solid contact may surround some regions (simply-connected cavities) which cannot be reached by the fluid. We then define  $\beta = \mathcal{M}(\Omega)/A_0$ , where  $\mathcal{M}(\Omega)$  is the measure of the fluid-flow domain  $\Omega$ . Of course  $\beta$  must satisfy the condition  $\beta \leq 1 - \alpha$ .

The shear stresses which the fluid exerts on the sliding surfaces can be written as

$$\tau^f = -\frac{s}{2}\nabla p \mp \mu \frac{\mathbf{U}_2 - \mathbf{U}_1}{s}, \quad (7)$$

where the upper sign (*minus*-sign) refers to the upper surface and the lower sign (*plus*-sign) to the lower surface. Note that the shear stress can be calculated from the velocity profile which, as predicted by the lubrication theory, is parabolic, and takes the form:

$$\mathbf{v}(\mathbf{x}, z) = -\frac{z(s-z)}{2\mu}\nabla p + \mathbf{U}_1\left(1 - \frac{z}{s}\right) + \mathbf{U}_2\frac{z}{s}.$$

The calculation of the average flow at the interface can be carried out by considering a generic representative elementary volume (REV),<sup>43</sup> also identified as the Tonder's *miniature bearing* at the contact interface.<sup>44</sup> The REV must be much larger than the largest roughness length-scale in order to include many realizations of the same roughness content, but much smaller than the macroscopic contact size to avoid to take into account the large-scale surface curvature. Under these conditions the local separation in the fluid domain  $\Omega$  can be written as:

$$s(\mathbf{x}, t) = u(\mathbf{x}, t) + h_r(\mathbf{x}, t) + w(\mathbf{x}, t), \quad (8)$$

where  $w(\mathbf{x}, t)$  is the sum of the local displacement due to the fluid-induced elastic deformation of both sliding surfaces, and  $h_r(\mathbf{x}, t)$  the sum of the heights of the (undeformed) roughness of the two surfaces, with  $\langle w(\mathbf{x}, t) \rangle = \langle h_r(\mathbf{x}, t) \rangle = 0$ . We observe that in the case of macroscopic steady-sliding, which is the focus of our investigation, the average interfacial separation in the REV is time-independent, *i.e.* one can write  $u(\mathbf{x}, t) \approx u(\mathbf{x})$ . Now assuming that  $h_r/u \ll 1$  we can write two second order terms in  $h_r/u$ ,<sup>45</sup>  $p \approx p_0 + p_1 + p_2$ , and

$$w(\mathbf{x}, t) \approx w_1(\mathbf{x}, t) + w_2(\mathbf{x}, t), \quad (9)$$

with the first and second order terms  $w_1(\mathbf{x}, t)$  and  $w_2(\mathbf{x}, t)$  satisfying the following equations:

$$w_1(\mathbf{x}, t) \approx \hat{K}[p_1(\mathbf{x}, t) - \langle p_1(\mathbf{x}, t) \rangle] \quad (10)$$

$$w_2(\mathbf{x}, t) \approx \hat{K}[p_2(\mathbf{x}, t) - \langle p_2(\mathbf{x}, t) \rangle], \quad (11)$$

where  $\hat{K}$  is a linear integral operator;

$$\hat{K}f(\mathbf{x}) = \int d^2x' K(\mathbf{x} - \mathbf{x}')f(\mathbf{x}'),$$

with the Fourier transform<sup>7</sup>  $K(q) = -2/(E^*q)$ , where  $q = |\mathbf{q}|$ . Assuming macroscopic steady-state conditions Eqn (8) can be rewritten as:

$$s(\mathbf{x}, t) = u(\mathbf{x}) + h(\mathbf{x}, t) + w_2(\mathbf{x}, t), \quad (12)$$

where  $h(\mathbf{x}, t) = w_1(\mathbf{x}, t) + h_r(\mathbf{x}, t)$  is a first order term separation. Expanding Eqn (6) we obtain:

$$\mathbf{J} \approx -\frac{u^3 + 3u^2h + 3u^2w_2 + 3h^2u}{12\mu}\nabla(p_0 + p_1 + p_2) + \mathbf{U}_m(u + h + w_2)$$

$$\approx \left(-\frac{u^3}{12\mu}\nabla p_0 + \mathbf{U}_m u\right) + \left(-\frac{u^3}{12\mu}\nabla p_1 - \frac{3u^2h}{12\mu}\nabla p_0 + \mathbf{U}_m h\right)$$

$$+ \left(-u^2\frac{u\nabla p_2 + 3h\nabla p_1}{12\mu} - \frac{3u^2w_2 + 3h^2u}{12\mu}\nabla p_0 + \mathbf{U}_m w_2\right), \quad (13)$$

and

$$\frac{\partial s}{\partial t} \approx \frac{\partial h}{\partial t} + \frac{\partial w_2}{\partial t}.$$

The continuity equation then gives:

$$\nabla^2 p_0 = 0$$

at the zero order, while at the first order<sup>45</sup> one obtains:

$$\frac{\partial h}{\partial t} - \frac{u^3}{12\mu}\nabla^2 p_1 - \frac{3u^2}{12\mu}\nabla h \cdot \nabla p_0 + \mathbf{U}_m \cdot \nabla h = 0 \quad (14)$$

(note then that since  $\langle h \rangle = 0$  we have  $\langle p \rangle = p_0 + \langle p_2 \rangle$ ). Taking the time and spatial Fourier transform of Eqn (14) one obtains:

$$p_1(\mathbf{q}, \omega) = ih(\mathbf{q}, \omega) \left[ \frac{3\mathbf{q} \cdot \nabla p_0}{uq^2} - \frac{12\mu(\omega + \mathbf{q} \cdot \mathbf{U}_m)}{u^3q^2} \right], \quad (15)$$

where  $\mathbf{q}$  is the wave-vector and  $\omega$  the pulsating frequency. Assuming that the two surfaces are sliding one against the other at different constant velocities  $\mathbf{U}_1$  and  $\mathbf{U}_2$  we can write  $h_r(\mathbf{x}, t) = h_{r1}(\mathbf{x} - \mathbf{U}_1 t) + h_{r2}(\mathbf{x} - \mathbf{U}_2 t)$  and in the frequency domain  $h_r(\mathbf{q}, \omega) = h_{r1}(\mathbf{q})\delta(\omega - \mathbf{q} \cdot \mathbf{U}_1) + h_{r2}(\mathbf{q})\delta(\omega - \mathbf{q} \cdot \mathbf{U}_2)$ . Moreover we can correlate  $p_1(\mathbf{q}, \omega)$  to  $w_1(\mathbf{q}, \omega)$  by taking the Fourier transform of Eqn (10). Thus, we obtain

$$w_1(\mathbf{q}, \omega) = K(q)p_1(\mathbf{q}, \omega). \quad (16)$$

We observe that for linearly viscoelastic solids, the term  $K(q)$  in Eqn (16) must be replaced with the corresponding viscoelastic response function.<sup>39</sup> Thus we can write:

$$h(\mathbf{q}, \omega) = h_{r1}(\mathbf{q})\delta(\omega - \mathbf{q} \cdot \mathbf{U}_1) + h_{r2}(\mathbf{q})\delta(\omega - \mathbf{q} \cdot \mathbf{U}_2) + K(q)p_1(\mathbf{q}, \omega). \quad (17)$$

Substituting Eqn (17) in Eqn (15) we find that the transform of the separation fluctuation (induced by the fluid action) can be written as:

$$h(\mathbf{q}, \omega) = [1 + K(q)G(\mathbf{q}, \omega)][h_{r1}(\mathbf{q})\delta(\omega - \mathbf{q} \cdot \mathbf{U}_1) + h_{r2}(\mathbf{q})\delta(\omega - \mathbf{q} \cdot \mathbf{U}_2)], \quad (18)$$

or equivalently

$$p_1(\mathbf{q}, \omega) = G(\mathbf{q}, \omega)[h_{r1}(\mathbf{q})\delta(\omega - \mathbf{q} \cdot \mathbf{U}_1) + h_{r2}(\mathbf{q})\delta(\omega - \mathbf{q} \cdot \mathbf{U}_2)],$$

where  $G(\mathbf{q}, \omega)$  describes the interaction between the fluid and the asperities (local fluid–structure interactions, IFSI) of the rough surfaces:

$$G(\mathbf{q}, \omega) = i \left[ \frac{3\mathbf{q} \cdot \nabla p_0}{uq^2} - \frac{12\mu(\omega + \mathbf{q} \cdot \mathbf{U}_m)}{u^3q^2} \right] \times \left[ 1 - iK(q) \left( \frac{3\mathbf{q} \cdot \nabla p_0}{uq^2} - \frac{12\mu(\omega + \mathbf{q} \cdot \mathbf{U}_m)}{u^3q^2} \right) \right]^{-1}. \quad (19)$$

It is interesting to note that Eqn (19) tends to  $[-K(q)]^{-1}$  for average separations close to zero, so that the transition from lubricated to boundary lubricated conditions occurs without loss of continuity. Note also that the fluid–wall interaction, due to the coupling between the sliding elastic walls and the viscous interposed fluid, introduces a phase-shift  $\varphi(\mathbf{q}, \omega)$  between the pressure field and sliding roughness pattern profiles, that can be calculated as:

$$\tan\varphi(\mathbf{q}, \omega) = \frac{\text{Im}G(\mathbf{q}, \omega)}{\text{Re}G(\mathbf{q}, \omega)} = -K^{-1}(q) \frac{u^3q^2}{3u^2\mathbf{q} \cdot \nabla p_0 - 12\mu(\omega + \mathbf{q} \cdot \mathbf{U}_m)}.$$

The average flow in  $\Omega$  can be calculated by averaging Eqn (13) to get:

$$\langle \mathbf{J} \rangle = -\frac{u^3}{12\mu} \nabla \langle p_0 + p_2 \rangle + \mathbf{U}_m u - \frac{u \langle h^2 \rangle}{4\mu} \nabla \langle p_0 + p_2 \rangle - \frac{u^2}{4\mu} \langle h \nabla p_1 \rangle, \quad (20)$$

since, to the 2nd order,  $\langle h^2 \rangle \langle p_0 \rangle = \langle h^2 \rangle \langle p_0 + p_2 \rangle$ . Observe that the average fluid pressure  $\langle p \rangle$ , corresponding to  $\langle p_0 + p_2 \rangle$ , is included in Eqn (20). However in the following, for the sake of a simplified notation, we will make use of the symbol  $p_0$  to identify  $\langle p \rangle$ . In order to determine  $\langle \mathbf{J} \rangle$  we need to calculate  $\langle h^2 \rangle$  and  $\langle h \nabla p_1 \rangle$ . This can be done by following the procedure shown in the Appendix A (see also Ref. 45). This leads to:

$$\langle h^2 \rangle = \sum_{i=1}^2 \langle h_i^2 \rangle = \varepsilon^s(\bar{u}) \sum_{i=1}^2 \int d^2q \frac{C_i(\mathbf{q})}{\lambda_i(\mathbf{q}, u, \nabla p_0)} \quad (21)$$

and

$$\langle h \nabla p_1 \rangle = -\varepsilon^s(\bar{u}) \sum_{i=1}^2 \int d^2q \left[ \mathbf{q} \frac{3\mathbf{q} \cdot \nabla p_0}{uq^2} - \mathbf{q} \frac{12\mu\mathbf{q} \cdot (\mathbf{U}_i + \mathbf{U}_m)}{u^3q^2} \right] \frac{C_i(\mathbf{q})}{\lambda_i(\mathbf{q}, u, \nabla p_0)}, \quad (22)$$

where  $\varepsilon^s(\bar{u})$  is given by Eqn (5), and where we defined the parameter  $\lambda_i$ , related to the intensity of the deformation induced

at the roughness scale by the fluid action on the  $i$ -th surface (the higher the  $\lambda_i$ , the higher the intensity of the deformation) as:

$$\lambda_i(\mathbf{q}, u, \nabla p_0) = 1 + \frac{36}{\zeta^4} \left[ \frac{1}{u/h_{\text{rms}}} \frac{\nabla p_0 \cdot \mathbf{q}}{q_0^2 h_{\text{rms}} E^*} \frac{\mathbf{q}}{q} - \frac{1}{u^3/h_{\text{rms}}^3} \frac{4\mu[2\mathbf{U}_m \pm \Delta\mathbf{U}] \cdot \mathbf{q}}{q_0^2 h_{\text{rms}}^3 E^*} \frac{\mathbf{q}}{q} \right]^2 \geq 1, \quad (23)$$

with  $\Delta\mathbf{U} = (\mathbf{U}_2 - \mathbf{U}_1)/2$ . In Eqn (23) the upper sign (*plus*-sign) refers to the upper solid surface (2) and the lower sign (*minus*-sign) to the bottom surface (1). The detailed derivation of Eqn (23) is presented in Appendix A. We can also define a IFSI parameter  $0 \leq \varepsilon_i^f \leq 1$ :

$$\varepsilon_i^f(u, \nabla p_0) = \int d^2q \frac{C_i(\mathbf{q})}{\lambda_i(\mathbf{q}, u, \nabla p_0)} \bigg/ \int d^2q C_i(\mathbf{q}) \quad (24)$$

from which  $\langle h_i^2 \rangle = \varepsilon^s(\bar{u}) \varepsilon_i^f(u, \nabla p_0) h_{\text{rms},i}^2$ . The effect of fluid–asperity interactions on the local separation is completely captured by the parameter  $\lambda_i(\mathbf{q}, u, \nabla p_0)$ . The amplitudes of the spectral components of the fluid film thickness  $s(\mathbf{x}, t)$  are given by the weighted sum of the spectral amplitudes of the original undeformed rough surfaces (where the weights are given by  $\lambda_i^{-1}$ ) multiplied by the smoothing parameter  $\varepsilon^s(\bar{u})$ , resulting in an average separation fluctuation  $\langle h^2 \rangle = \varepsilon^s(\bar{u}) \varepsilon_1^f h_{\text{rms},1}^2 + \varepsilon_2^f h_{\text{rms},2}^2$ . The presence of the local squeeze motions, combined to the viscous action coming from the flow driving term  $\mathbf{U}_m$ , determines different  $\lambda_i$  parameters for the two surfaces.

The  $ms$  roughness  $\langle h_i^2 \rangle$  of the  $i$ -th surface (where (1) is for the bottom surface and (2) is for the upper surface) is generally different from the value  $\langle h_i^2 \rangle$ . Indeed,  $\langle h_i^2 \rangle$  represents the contribution of the  $i$ -th surface in term of effective  $ms$  separation to the average fluid flow, whereas the true  $ms$  roughness  $\langle h_i^2 \rangle$  of the  $i$ -th surface can be calculated (at the first order) from:

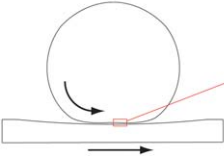

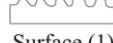
$$h_i(\mathbf{q}, \omega) = h_{r,i}(\mathbf{q})\delta(\omega - \mathbf{q} \cdot \mathbf{U}_i) + p_1(\mathbf{q}, \omega)K_i(q),$$

where  $K_i(q) = K(q)E^*/E_i^*$  and  $E_i^* = E_j/(1 - \nu_i^2)$ . By using a similar approach as the one presented in Appendix A we get:

$$\langle h_i^2 \rangle = \langle h_i^2 \rangle + \varepsilon^s(\bar{u}) \left( \frac{E^*}{E_i^*} \right)^2 \int d^2q C_i(\mathbf{q}) \frac{\lambda_i(\mathbf{q}, u, \nabla p_0) - 1}{\lambda_i(\mathbf{q}, u, \nabla p_0)} + \varepsilon^s(\bar{u}) \left( \frac{E^*}{E_i^*} \right)^2 \int d^2q C_j(\mathbf{q}) \frac{\lambda_j(\mathbf{q}, u, \nabla p_0) - 1}{\lambda_j(\mathbf{q}, u, \nabla p_0)}, \quad (25)$$

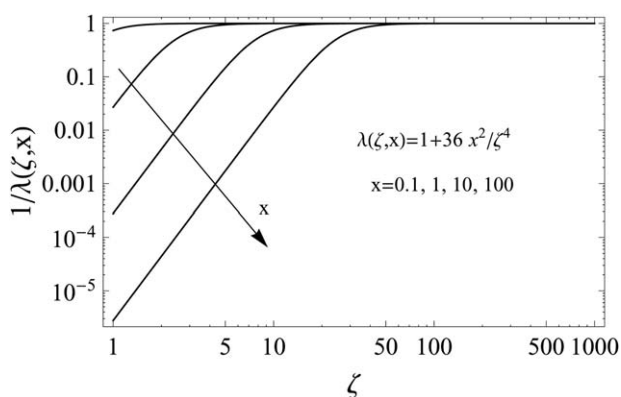
where  $j = 3 - i$ , and  $i = 1$  or  $i = 2$ . Note that  $\langle h^2 \rangle_i \geq \langle h_i^2 \rangle$ . In Table 1 we show the  $ms$  roughness  $\langle h_i^2 \rangle$  and the  $ms$  separation  $\langle h_i^2 \rangle$  of the surface  $i$ -th in a comparison chart, for the simple case of a smooth surface (2) in sliding contact with a rough substrate (1), characterized by a rms roughness  $h_{\text{rms}}$ . Four cases are considered: (i) both surfaces are compliant (*e.g.* tongue–palate contact), (ii) surface (1) compliant and (2) rigid (*e.g.* rubber seal–shaft contact), (iii) surface (1) rigid and (2) compliant (*e.g.* tire–road or cell–substrate contact), (iv) both surfaces rigid. For all cases we have, from Eqn (21), a  $ms$  separation  $\langle h_i^2 \rangle = 0$ . However, when surface (2) is compliant we have  $\langle h_2^2 \rangle \geq 0$ , which means that a non zero roughness is generated on (2). In particular, in case (iii) the rough surface is rigid and then  $\langle h_1^2 \rangle = \varepsilon^s h_{\text{rms}}^2$  as expected, whereas, due to the local fluid pressure fluctuations generated by surface (1), surface (2) gains a  $ms$

**Table 1** Comparison chart.  $\langle h_i^2 \rangle$  and  $\langle h_i'^2 \rangle$  have been calculated for the case of a smooth surface (2) in sliding contact with a rough substrate (1) with rms roughness  $h_{\text{rms}}$

Macroscopic contact geometry		REV	Surface (1)	
		Surface (2)  Surface (1) 	Compliant	Rigid
Surface (2)	Compliant	$\langle h_1^2 \rangle \geq \varepsilon^s \varepsilon_1^f h_{\text{rms}}^2$ $\langle h_2^2 \rangle = \langle h_1^2 \rangle - \varepsilon^s \varepsilon_1^f h_{\text{rms}}^2$ $\langle h_1'^2 \rangle = \varepsilon^s \varepsilon_1^f h_{\text{rms}}^2$	$\langle h_1^2 \rangle = \varepsilon^s h_{\text{rms}}^2$ $\langle h_2^2 \rangle = \langle h_1^2 \rangle (1 - \varepsilon_1^f)$ $\langle h_1'^2 \rangle = \varepsilon^s \varepsilon_1^f h_{\text{rms}}^2$	
	Rigid	$\langle h_1^2 \rangle = \varepsilon^s \varepsilon_1^f h_{\text{rms}}^2$ $\langle h_2^2 \rangle = 0$ $\langle h_1'^2 \rangle = \varepsilon^s \varepsilon_1^f h_{\text{rms}}^2$	$\langle h_1^2 \rangle = h_{\text{rms}}^2$ $\langle h_2^2 \rangle = 0$ $\langle h_1'^2 \rangle = h_{\text{rms}}^2$	

roughness  $\langle h_2^2 \rangle = \langle h_1^2 \rangle (1 - \varepsilon_1^f)$ . Note that in the limiting case of  $\bar{u}/h_{\text{rms}} \ll 1$  (and non zero sliding velocity), the intensity of the fluid–asperity interactions is maximized ( $\varepsilon_1^f \rightarrow 0$ ) resulting in  $\langle h_2^2 \rangle \rightarrow \langle h_1^2 \rangle$ . This is easy to understand if we consider that for  $\bar{u}/h_{\text{rms}} \ll 1$  a very thin lubricant layer covers the non contact areas, so that the local profiles of both surfaces in those domains differ by less than a constant, the latter being the thickness of the lubricant layer. Therefore we must have  $\langle h_2^2 \rangle \approx \langle h_1^2 \rangle$ . In case (ii) the rough surface is compliant. In such conditions  $\langle h_1^2 \rangle = \langle h_1'^2 \rangle = \langle h^2 \rangle = \varepsilon^s \varepsilon_1^f h_{\text{rms}}^2$  so that the separation fluctuation coincides with the fluctuation of the surface roughness. For the latter contact configuration the IFSI coefficient  $\varepsilon_1^f$  is more likely to be a viscous flattening coefficient, since it directly links the average flattening undergone by the surface asperities as a consequence of the fluid pressure fluctuations caused by the same roughness.

In Fig. 3 we show how  $\lambda_i^{-1}$  varies as a function of the magnification  $\zeta = |q|/q_0$ . We write  $\lambda = 1 + 36x^2/\zeta^4$ , where  $x$  represents the content of the square brackets in Eqn (23). Note that, as documented in Refs. 22–24, the high frequency roughness is almost unchanged by the viscous action, while the large wavelengths components are strongly affected; this is again in agreement with the existing experimental evidence.



**Fig. 3** The intensity of the fluid–asperity interactions, expressed in terms of  $1/\lambda$ , as a function of magnification.

This local viscous action is determined by the superposition of three effects which can be identified by three dimensionless parameters: (i) the Poiseuille parameter  $\mathbf{F}_P = \nabla p_0 / (q_0^2 h_{\text{rms}}^2 E^*)$ , related to the intensity of the fluid–asperity interactions due to the pressure gradient, (ii) the sliding parameter  $\mathbf{F}_S = 4\mu\Delta\mathbf{U} / (q_0^2 h_{\text{rms}}^3 E^*)$  and (iii) the rolling parameter  $\mathbf{F}_R = 8\mu\mathbf{U}_m / (q_0^2 h_{\text{rms}}^3 E^*)$ , which govern that part of  $\varepsilon_1^f$  caused by the sliding and rolling components of motion. Eqn (23) can be rewritten as:

$$\lambda_i(\mathbf{q}, u, \nabla p_0) = 1 + \frac{36}{\zeta^4} \left[ \frac{\mathbf{F}_P \cdot \mathbf{q}/q}{u/h_{\text{rms}}} - \frac{\mathbf{F}_R \cdot \mathbf{q}/q}{(u/h_{\text{rms}})^3} \mp \frac{\mathbf{F}_S \cdot \mathbf{q}/q}{(u/h_{\text{rms}})^3} \right]^2,$$

where the upper sign (*minus*-sign) refers to the upper solid surface (2) and the lower sign (*plus*-sign) to the bottom surface (1). Note that while the pressure gradient term  $\mathbf{F}_P$  term has a factor proportional to the dimensionless ratio  $h_{\text{rms}}/u$ , the  $\mathbf{F}_S$  and  $\mathbf{F}_R$  contributions to IFSI are weighted with the cube of  $h_{\text{rms}}/u$ . We also note that the IFSI are strongly directional dependent, being much more effective for the roughness wave-components aligned with  $\mathbf{F}_P$ ,  $\mathbf{F}_S$  and  $\mathbf{F}_R$ .

Eqn (22) can be arranged in terms of the anisotropy tensor  $\mathbf{D}(u, \nabla p_0)$ ,<sup>45</sup> which in our case obeys the following relations:

$$\begin{aligned} \langle h^2 \rangle \mathbf{D}(u, \nabla p_0) &= \sum_{i=1}^2 \langle h_i^2 \rangle \mathbf{D}_i(u, \nabla p_0) \\ \langle h_i^2 \rangle \mathbf{D}_i(u, \nabla p_0) &= \varepsilon^s(\bar{u}) \int d^2 q \frac{\mathbf{q}\mathbf{q}}{q^2} \frac{C_i(\mathbf{q})}{\lambda_i(\mathbf{q}, u, \nabla p_0)}, \end{aligned} \quad (26)$$

where the index  $i = 2$  is for the upper surface and  $i = 1$  for the bottom surface. The average fluid–asperity interaction can be then expressed as:

$$\langle h \nabla p_1 \rangle = \frac{12\mu}{u^3} \sum_{i=1}^2 \mathbf{D}_i \mathbf{U}_i \langle h_i'^2 \rangle - \frac{3}{u} \langle h^2 \rangle \mathbf{D} \nabla p_0 + \frac{12\mu}{u^3} \langle h^2 \rangle \mathbf{D} \mathbf{U}_m \quad (27)$$

and the average flow vector  $\langle \mathbf{J} \rangle$  can be calculated as:

$$\langle \mathbf{J} \rangle \approx -\frac{\bar{u}}{12\mu} \frac{1}{\beta} \Phi_P \nabla p_0 + \bar{u} \frac{1}{\beta} \Phi_S \mathbf{U}_m - \bar{u} \sum_{i=1}^2 \frac{1}{\beta} \Phi_T \mathbf{U}_i, \quad (28)$$

where we have defined the flow factors tensors as:

$$\begin{aligned}\frac{(1-\alpha)^3}{\beta}\Phi_P &= \mathbf{I} + \frac{3\langle h^2 \rangle}{u^2}\mathbf{I} - \frac{9\langle h^2 \rangle}{u^2}\mathbf{D} \\ \frac{1-\alpha}{\beta}\Phi_S &= \mathbf{I} - 3\frac{\langle h^2 \rangle}{u^2}\mathbf{D} \\ \frac{1-\alpha}{\beta}\Phi_{T_i} &= \frac{3\langle h_i^2 \rangle}{u^2}\mathbf{D}_i,\end{aligned}\quad (29)$$

and where  $\Phi_P = \Phi_P(\bar{u}, \nabla p_0)$  is the pressure flow factor tensor,  $\Phi_S = \Phi_S(\bar{u}, \nabla p_0)$  the shear flow factor tensor and  $\Phi_{T_i} = \Phi_{T_i}(\bar{u}, \nabla p_0)$  the squeeze flow factor tensor, all depend upon both the average interfacial separation  $\bar{u}$  and the pressure gradient  $\nabla p_0$ , and therefore cannot be determined *a priori* without solving the entire lubrication problem. The anisotropy tensors  $\mathbf{D}_i$  link the anisotropic characteristics of a generic roughness to the flow conductivity tensors of the contact interface. In the ideal case of rigid and isotropic surfaces  $\mathbf{D}_i = \mathbf{I}/2$  and, consequently, the generic flow factor tensor  $\Phi_i \propto \mathbf{I}$ . This directly results in an isotropic flow conductivity, *e.g.* by considering as driving term the only fluid pressure gradient, the flow term becomes  $\langle \mathbf{J} \rangle \propto \Phi_P \nabla p_0 \propto \nabla p_0$ . However, in the most general case, the flow at the interface is not directed along the driving sources (*e.g.* the fluid pressure gradient), since the surfaces roughness effectively redirects the fluid particles along some resultant (average) direction. The latter is uniquely determined through the anisotropic tensors.

We stress that, as shown in Eqn (28), the asperity–asperity interactions as well as the fluid–asperity interactions have a key role in the formation of the average fluid flow, both in magnitude (through the quantities  $\langle h_i^2 \rangle$ ) and in direction (through the tensors  $\mathbf{D}_i$ ). It is also interesting to note that the average flow direction, governed by elements of  $\mathbf{D}$ , is given by the *rms*-weighted average of the anisotropy tensors of each surface, which means that in the sliding between rough surfaces with very different *rms*-roughness, the intensity and direction of the flow is mainly determined by the rougher surface.

The average or macroscopic fluid dynamics equation follows from the mass conservation law. Recalling that  $\mathbf{n} \cdot \mathbf{J} = 0$  at the boundaries  $\partial\Omega$ , one can show that:

$$\langle \nabla \cdot \mathbf{J} \rangle_{A_0} = \nabla \cdot \langle \mathbf{J} \rangle_{A_0} \quad (30)$$

with  $\langle \mathbf{J} \rangle_{A_0} = A_0^{-1} \int_{\Omega} \mathbf{J} dA = [\mathcal{M}(\Omega)/A_0] \langle \mathbf{J} \rangle = \beta \langle \mathbf{J} \rangle$ , where

$\langle \mathbf{J} \rangle = [\mathcal{M}(\Omega)]^{-1} \int_{\Omega} \mathbf{J} dA$  has been previously calculated. Using

Eqns (28) and (30) the average Reynolds equation for macroscopically steady sliding contacts becomes:

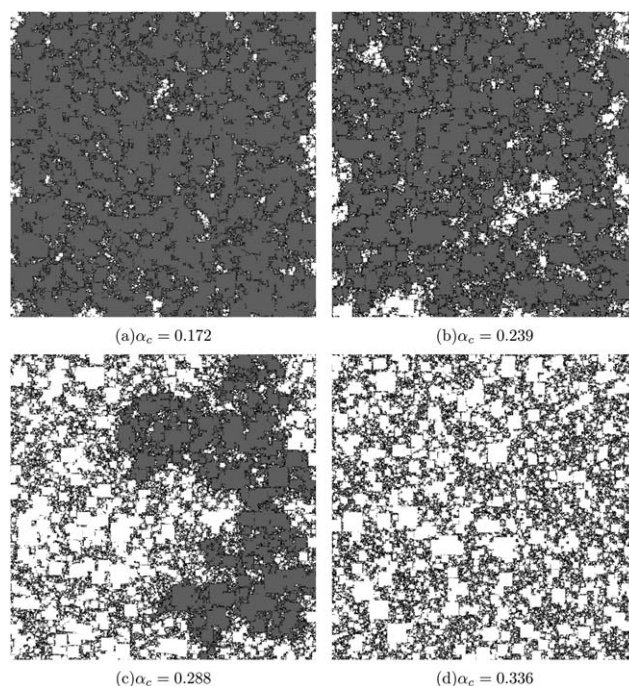
$$\nabla \cdot \left[ \frac{\bar{u}^3}{12\mu} \Phi_P \nabla p_0 \right] = \nabla \cdot [\bar{u} \Phi_S \mathbf{U}_m] - \nabla \cdot [\bar{u} \Phi_{T_i} \mathbf{U}_i], \quad (31)$$

where we used  $u = \bar{u}/(1-\alpha)$ , and where  $\Phi_i = \Phi_i(\bar{u}, \nabla p_0)$  are calculated from Eqn (29).

#### IV. On the size of fluid-flow domain

We now turn our attention to the quantity,  $\beta = \mathcal{M}(\Omega)/A_0$ , defined as the normalized fluid flow area, given by the ratio

between the amount of the non contact areas occupied by the lubricant in the REV, and the total REV area  $A_0$ . Note first that the difference between the normalized fluid flow area,  $\beta$ , and the normalized area of non contact,  $1-\alpha$ , can be mainly attributed to the presence of simply-connected voids surrounded by solid–solid contact walls that cannot be reached by the fluid or (in case fluid is already present) where it cannot escape from. Fig. 4 (calculated with the percolation model developed in Ref. 46) clearly shows what happens in a deterministic realization of the contact interface: the numerically calculated fluid flow domain area (gray) is shown for different values of the solid contact area (black). Note that the more the area of contact is increased, the more the fluid flow area is different from the total non contact area. We observe that at  $\alpha \approx 0.34$  the fluid flow area vanishes, although free voids are still present at the interface. This interesting effect, which has so far been investigated only for static seals,<sup>16–18,46</sup> is determined by the occurrence of two-dimensional contact geometries at the interface, which behave like solid walls that prevent fluid flow through the voids. Even for small percentages of the contact area (see Fig. 4(a)) some simply connected voids still exist which do not contribute to fluid flow. What happens is that at small values of  $\alpha$  (see Fig. 4(a)), the contact area increases mainly by the nucleation of new contact patches (we call this the nucleation regime), which are expected to be almost equally distributed at the interface. The average flow resistivity then increases essentially because the stream lines of the fluid flow must bypass the solid–solid contact area thus increasing the hydraulic losses. By increasing the contact area, the newly formed contacts start to coalesce and merge with the already existing ones; this process first happens gradually (see Fig. 4(a) and 4(b)), and then accelerates (see Fig. 4(c) and 4(d)) in



**Fig. 4** Numerical prediction of the normalized fluid area  $\beta$ . Black, white and gray domains correspond, respectively, to contact, non contact and fluid areas. Calculated with the percolation model described in Ref. 46.



the proximity to the percolation threshold. During this coalescence stage the size of the voids increases, determining the further increase of the average flow resistivity due to the strong decrease of the amount of fluid filled areas (there are less paths available to the fluid to flow through the voids).

There is a second reason for which  $\beta$  may differ from  $1 - \alpha$ , related to local dewetting transitions.<sup>47–49</sup> However, in this work we have not considered surface energies contributions, thus  $\beta$  comes exclusively from geometric effects.

In Fig. 5 we show the apparent area of contact which occurs when the interface is observed at the magnification  $\zeta$  (Fig. 5(a)), and the same apparent contact patches at the highest magnification  $\zeta_1 = q_1/q_0$ , *i.e.*, when all the roughness is included in the contact (Fig. 5(b)). We note that the real contact area in Fig. 5(b) is only a fraction of the apparent contact areas shown in Fig. 5(a). It is possible to determine this fraction by considering that the average pressure in the apparent contact area  $A(\zeta)$  is just the total applied force divided by  $A(\zeta)$ , namely  $[A_0/A(\zeta)]\sigma_0$ , and recalling that at magnification  $\zeta$  only roughness components with wave vector  $q > q_0\zeta$  will affect the real contact area, one obtains using Eqn (1):

$$\frac{\tilde{A}(\zeta)}{A(\zeta)} = \text{erf}\left(\frac{\sqrt{2}}{E^*[\nabla h]_{\text{rms}}(\zeta)} \frac{A_0}{A(\zeta)} \sigma_0\right), \quad (32)$$

where this time  $[\nabla h]_{\text{rms}}(\zeta)$  is the *rms* roughness slope including only the roughness components with wavevector  $q_1 > |q| > q_0\zeta$ :

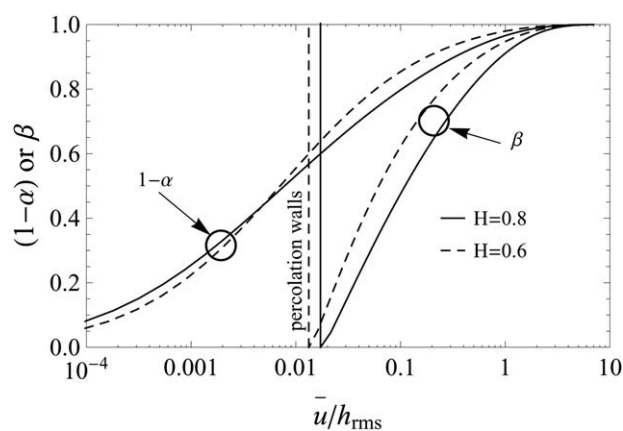
$$[\nabla h]_{\text{rms}}^2(\zeta) = \int_{q_1 > |q| > q_0\zeta} d^2q C(q) q^2. \quad (33)$$

Note that Eqn (32) reduces to one for  $\zeta = \zeta_1$ .

It is observed that if the relative contact area  $\tilde{A}(\zeta)/A(\zeta)$ , in the apparent contact patches of Fig. 5(a), is larger than the area given by the percolation threshold (about 0.4),<sup>50</sup> then the newly formed voids shown in Fig. 5(b) (although they may be in principle partially filled with lubricant), cannot contribute to the average flow since the contact “labyrinths” (black areas) surrounding these voids behave like impenetrable walls. Therefore, more rigorously  $\beta$  should be defined as  $\beta = 1 - A(\zeta_p)/A_0$  where the magnification threshold  $\zeta_p$  must be the magnification at which the (normalized) real area of contact occurring in the apparent contact patches at  $\zeta = \zeta_p$  is equal to the area at which percolation starts that, for isotropic roughness, requires  $\tilde{A}(\zeta_p)/A$



**Fig. 5** The role of percolation at the contact interface (schematic). (a) Area of contact as it appears when the contact is observed at the magnification  $\zeta$ . (b) The real area of contact (observed at the highest magnification  $\zeta_1$ ) corresponding to Fig. 5(a).



**Fig. 6** The quantities  $\beta$  and  $1 - \alpha$  as functions of the average interfacial separation. For  $\zeta_1 = 1000$ ,  $H = 0.6$  and  $H = 0.8$ .

( $\zeta_p$ )  $\approx \alpha_p^{\nu}$ . In the general case of anisotropic surfaces,  $\zeta_p$  should depend on the flow direction angle  $\theta$  and so does  $\beta$ , which can therefore be written in a general form as  $\beta = \beta(\sigma_0, \theta)$ . Here we discuss only the isotropic case, and select  $\alpha_p^{\nu} = 0.4$ ,<sup>16</sup> despite having been shown<sup>50</sup> that the (average) percolation threshold  $\alpha_p^{\nu}$  should depend on the magnification  $\zeta$  as a power law ( $\alpha_p^{\nu} - \alpha_p^{\nu}$ )  $\propto \zeta^{1/\nu}$  (where the exponent  $\nu$  can be determined by numerical percolation calculations). The effect of the contact magnification  $\zeta$  on the percolation threshold value is actually under investigation by some of the authors, and will be presented in a dedicated paper.<sup>46</sup> In Fig. 6 we show our model prediction  $\beta$  compared with the non-contact area  $1 - \alpha$  as a function of the average interfacial separation in the case of self affine isotropic roughness with  $\zeta_1 = 1000$  and two Hurst exponents, 0.6 and 0.8. Note that the nucleation regime occurs for dimensionless separation  $\bar{u}/h_{\text{rms}} \geq 1$ , since the difference between  $\beta$  and  $1 - \alpha$  is very small in that zone. The coalescence regime occurs instead in a range of separation  $0.01 < \bar{u}/h_{\text{rms}} < 1$ , where the normalized fluid area starts to strongly deviate from the normalized non contact area. Interestingly,  $\beta$  vanishes at the percolation threshold, after which a further decrease of separation is not relevant since the fluid flow cannot occur despite the large amount of free voids at the interface.

## V. The average solids deformation

In order to close the set of equations needed to solve the mixed lubrication problem we need to also calculate the macroscopic deformations of the solids due to the locally averaged normal stress (the sum of the solid and fluid pressure)  $\sigma_T = \sigma_0 + \beta p_0$ . The total stress  $\sigma_T$  can easily be related to the local average separation  $\bar{u}(\mathbf{x})$  through the macroscopic contact geometry equation:

$$\bar{u}(\mathbf{x}) = \bar{u}_R(0) + f(\mathbf{x}) + w(\mathbf{x}), \quad (34)$$

where  $w(\mathbf{x})$  is the average elastic displacement, determined from:

$$w(\mathbf{x}) = \int d^2x' K(\mathbf{x} - \mathbf{x}') \sigma_T(\mathbf{x}'). \quad (35)$$

$K(\mathbf{x})$  is the Green function of the elastic solids given by the Boussinesq solution  $K(\mathbf{x}) = [\pi E^* |\mathbf{x}|]^{-1}$ , and  $f(\mathbf{x})$  is the shape of the

interfacial separation assuming the two surfaces are not deformed (e.g.  $f(\mathbf{x}) = R - \sqrt{R^2 - |\mathbf{x}|^2}$  for a ball of radius  $R$  on a flat substrate).  $\bar{u}_R(0)$  is a constant which simply represents the central distance between the two surfaces assuming they are not deformed. We also need the global force-balance equation along the normal direction which gives:

$$\int dA \sigma_T(\mathbf{x}) = F_N. \quad (36)$$

Moreover, the total applied shear stress  $\tau = \tau^s + \tau^f$ , where the latter is calculated as shown in Appendix B.

## VI. Conclusions

In this paper we have proposed a novel theory to describe the transition from the hydrodynamic lubrication to the boundary lubrication regime occurring in soft contacts. Our approach is of a mean field type and based on a perturbation treatment, which enables the consistent calculation of both asperity–asperity and asperity–fluid interactions and their effects on the average fluid flow and solid contact mechanics at the interface. In particular, we have derived the flow factors including elastic deformation, which turn out to depend not only on the interfacial separation  $\bar{u}$ , but also on the fluid pressure gradient  $\nabla p_0$ , to be determined as a part of the solution of the homogenized system of equations governing the lubricated contact problem. The proposed methodology is useful in investigating lubrication problems ranging from boundary to hydrodynamic lubrication regimes, and in particular should allow to elucidate the contact and lubrication mechanisms which occur when only part of the interface is occupied by the fluid. These aspects are discussed in details in the companion Part II.<sup>36</sup>

## Nomenclature

$\nu_i$	Poisson's ratio
$\alpha_\infty^p$	Normalized area of percolation for an infinitely sized representative elementary volume
$\alpha_\zeta^p$	Normalized area of percolation at the magnification $\zeta$
$\alpha$	Normalized area of solid contact
$\bar{u}$	Average interfacial separation
$\beta$	Normalized area of fluid flow
$\langle h_i^2 \rangle$	Mean square separation fluctuation related to surface $i$ -th
$\langle h_i^2 \rangle$	Mean square roughness of surface $i$ -th
$\langle h^2 \rangle$	Mean square separation fluctuation
$\Phi_i$	Flow factor tensor
$\mathbf{D}_i$	Anisotropy tensor
$\mathbf{I}$	Identity matrix
$\mathbf{T}_i$	Shear stress tensor
$\mathbf{U}_m$	Mean velocity $(\mathbf{U}_1 + \mathbf{U}_2)/2$
$\mathbf{U}_i$	Surface velocity
$\mu$	Fluid viscosity
$\omega$	Time frequency
$\sigma_0$	Average solid contact pressure
$\sigma_T$	Average pressure on $A_0$

$\tau^f$	Fluid wall shear stress
$\tau^s$	Solid contact wall shear stress
$\varepsilon_i^f$	Fluid–asperity interaction parameter related to surface $i$ -th
$\varepsilon^s$	Smoothing parameter from solid contact
$\zeta = q/q_0$	Contact magnification
$A(\zeta)$	Area of solid contact at the magnification $\zeta$
$A_0$	Representative area of interaction
$A_c$	Area of solid contact in $A_0$
$A_n$	Area non contact in $A_0$
$C(q)$	Power spectral density
$E^*$	Reduced elastic modulus
$E_i$	Young's modulus
$G(\mathbf{q}, \omega)$	Fluid-asperity interaction kernel
$p_0$	Zero order fluid pressure
$p_1$	1st order fluid pressure
$p_2$	2nd order fluid pressure
$q$	Spatial wave vector
$q_0$	Large scale roughness cut-off frequency
$q_1$	Small scale roughness cut-off frequency
$u$	Average separation in the non contact areas
$w(\mathbf{x})$	Average displacement field

## Appendix A: Calculations of the film thickness fluctuation and of the average fluid asperity interaction

Eqn (21) can be determined as following. Consider the following equality (coming from the definition of power spectral density):

$$\langle h^2 \rangle = \varepsilon^s(\bar{u}) \int \int d^2q d^2q' \int \int d\omega d\omega'$$

$$\langle h(\mathbf{q}, \omega) h(\mathbf{q}', \omega') \rangle e^{i(\omega+\omega')t} e^{i(\mathbf{q}+\mathbf{q}')\cdot\mathbf{x}}.$$

For an homogeneous statistical process  $\phi(\mathbf{x})$  we have  $\langle \phi(\mathbf{q}) \phi(\mathbf{q}') \rangle = C_\phi(\mathbf{q}) \delta(\mathbf{q} + \mathbf{q}')$ . Thus, using Eqn (18) we can rewrite  $\langle h(\mathbf{q}, \omega) h(\mathbf{q}', \omega') \rangle$ :

$$\langle h(\mathbf{q}, \omega) h(\mathbf{q}', \omega') \rangle = \delta(\mathbf{q} + \mathbf{q}') \sum_{i=1}^2 \delta(\omega - \mathbf{q} \cdot \mathbf{U}_i) \delta(\omega' - \mathbf{q}' \cdot \mathbf{U}_i) C_i(\mathbf{q})$$

$$\times [1 + K(q)G(\mathbf{q}, \omega)][1 + K(q')G(\mathbf{q}', \omega')],$$

so that:

$$\langle h_i^2 \rangle = \varepsilon^s(\bar{u}) \int d^2q [1 + K(q)G(\mathbf{q}, \mathbf{q} \cdot \mathbf{U}_i)]^2 C_i(\mathbf{q})$$

and  $\langle h^2 \rangle = \langle h_1^2 \rangle + \langle h_2^2 \rangle$ , where we defined  $\lambda_i(\mathbf{q}, u, \nabla p_0)$ :

$$\frac{1}{\lambda_i(\mathbf{q}, u, \nabla p_0)} = |1 + K(q)G(\mathbf{q}, \mathbf{q} \cdot \mathbf{U}_i)|^2.$$

Eqn (22) can be obtained by considering the following equality:

$$\langle h \nabla p_1 \rangle = \varepsilon^s(\bar{u}) \int \int d^2q d^2q' \int \int d\omega d\omega' (i\mathbf{q}) \langle p_1(\mathbf{q}, \omega) h(\mathbf{q}', \omega') \rangle e^{i(\omega+\omega')t} e^{i(\mathbf{q}+\mathbf{q}')\cdot\mathbf{x}}.$$

We then rewrite  $\langle p_1(\mathbf{q}, \omega) h(\mathbf{q}', \omega') \rangle$  with Eqns (18) and (19):

$$\langle p_1(\mathbf{q}, \omega) h(\mathbf{q}', \omega') \rangle = \delta(\mathbf{q} + \mathbf{q}') \sum_{i=1}^2 \delta(\omega - \mathbf{q} \cdot \mathbf{U}_i) \delta(\omega' - \mathbf{q}' \cdot \mathbf{U}_i) C_i(\mathbf{q}) \times G(\mathbf{q}, \omega) [1 + K(q') G(\mathbf{q}', \omega')],$$

and finally:

$$\begin{aligned} \langle h \nabla p_1 \rangle &= i \varepsilon^s(\bar{u}) \sum_{i=1}^2 \int d^2 q \mathbf{q} G(\mathbf{q}, \mathbf{q} \cdot \mathbf{U}_i) [1 + K(q) G(-\mathbf{q}, -\mathbf{q} \cdot \mathbf{U}_i)] C_i(\mathbf{q}) \\ &= -\varepsilon^s(\bar{u}) \sum_{i=1}^2 \int d^2 q \left[ \mathbf{q} \frac{3\mathbf{q} \cdot \nabla p_0}{u q^2} - \mathbf{q} \frac{12\mu \mathbf{q} \cdot (\mathbf{U}_i + \mathbf{U}_m)}{u^3 q^2} \right] \frac{C_i(\mathbf{q})}{\lambda_i(\mathbf{q}, u, \nabla p_0)}, \end{aligned}$$

where:

$$\begin{aligned} i \left[ \frac{3\mathbf{q} \cdot \nabla p_0}{u q^2} - \frac{12\mu \mathbf{q} \cdot (\mathbf{U}_i + \mathbf{U}_m)}{u^3 q^2} \right] / \lambda_i(\mathbf{q}, u, \nabla p_0) \\ = G(\mathbf{q}, \mathbf{q} \cdot \mathbf{U}_i) [1 + K(q) G(-\mathbf{q}, -\mathbf{q} \cdot \mathbf{U}_i)]. \end{aligned}$$

## Appendix B. The homogenized interfacial stress

By adopting the same procedure outlined in the previous section, the 2nd order expansion of shear stresses acting on the walls is:

$$\begin{aligned} \tau^f &\approx -\frac{u+h+w_2}{2} \nabla(p_0 + p_1 + p_2) \mp \mu \frac{\mathbf{U}_2 - \mathbf{U}_1}{u+h+w_2} \\ &= \left( -\frac{u}{2} \nabla p_0 \mp \mu \frac{\mathbf{U}_2 - \mathbf{U}_1}{u} \right) \\ &+ \left( -\frac{h}{2} \nabla p_0 - \frac{u}{2} \nabla p_1 \pm \mu h \frac{\mathbf{U}_2 - \mathbf{U}_1}{u^2} \right) \\ &+ \left( -\frac{h}{2} \nabla p_1 \mp \mu h^2 \frac{\mathbf{U}_2 - \mathbf{U}_1}{u^3} \pm \mu w_2 \frac{\mathbf{U}_2 - \mathbf{U}_1}{u^2} \right), \end{aligned}$$

where the upper sign is for the upper surface and the lower sign for the lower surface. The average shear stresses ( $\tau^f$ ) in the fluid flow region can be calculated:

$$\begin{aligned} \langle \tau^f \rangle &= -\frac{u}{2} \nabla p_0 - \frac{\langle h \nabla p_1 \rangle}{2} \mp \mu \frac{\mathbf{U}_2 - \mathbf{U}_1}{u} \left( 1 + \frac{\langle h^2 \rangle}{u^2} \right) \\ &= -\frac{\bar{u}}{2} \frac{1}{\beta} \mathbf{T}_R \nabla p_0 \mp \frac{1}{\beta} \mu \mathbf{T}_S \frac{\mathbf{U}_2 - \mathbf{U}_1}{\bar{u}} - \frac{\mu}{\bar{u}} \frac{1}{\beta} \sum_{i=1}^2 \mathbf{T}_{T_i} (\mathbf{U}_m + \mathbf{U}_i), \end{aligned} \quad (\text{B1})$$

where we have defined the rolling shear stress tensor  $\mathbf{T}_R = \mathbf{T}_R(\bar{u}, \nabla p_0)$ , the sliding shear stress tensor  $\mathbf{T}_S = \mathbf{T}_S(\bar{u}, \nabla p_0)$  and the squeeze shear stress tensor  $\mathbf{T}_{T_i} = \mathbf{T}_{T_i}(\bar{u}, \nabla p_0)$  such that:

$$\begin{aligned} \frac{1-\alpha}{\beta} \mathbf{T}_R &= \left[ \mathbf{I} - \frac{3\langle h^2 \rangle}{u^2} \mathbf{D} \right] \\ \frac{1}{(1-\alpha)\beta} \mathbf{T}_S &= \left[ \mathbf{I} + \frac{\langle h^2 \rangle}{u^2} \mathbf{I} \right] \\ \frac{1}{(1-\alpha)\beta} \mathbf{T}_{T_i} &= \left[ 6 \frac{\langle h_i^2 \rangle}{u^2} \mathbf{D}_i \right]. \end{aligned} \quad (\text{B2})$$

Finally the average fluid wall shear stress  $\tau^f = \langle \tau^f \rangle_{A_0}$  on the nominal contact area  $A_0$  can be calculated by taking the product of Eqns (B1) with  $\beta$  to get:

$$\tau^f = -\frac{\bar{u}}{2} \mathbf{T}_R \nabla p_0 \mp \mu \mathbf{T}_S \frac{\mathbf{U}_2 - \mathbf{U}_1}{\bar{u}} - \frac{\mu}{\bar{u}} \sum_{i=1}^2 \mathbf{T}_{T_i} (\mathbf{U}_m + \mathbf{U}_i),$$

where  $\mathbf{T}_i = \mathbf{T}_i(\bar{u}, \nabla p_0)$  are calculated from Eqns (B2) and where the upper sign is for the upper surface and the lower sign for the

lower surface. We note that the average frictional stress at wall  $\tau^f$  generally differs from  $\tau^f$ , since it includes the contributions of fluid pressure gradient at the interface and it can be easily calculated once the deformed contacting surfaces have been determined. In the simplest case of a smooth rigid (lower) surface in contact with a rough compliant (upper) surface it is easy to show:

$$\tau^f = \pm \frac{\bar{u}}{2} \mathbf{T}_R \nabla p_0 \mp \mu \mathbf{T}_S \frac{\mathbf{U}_2 - \mathbf{U}_1}{\bar{u}} \pm \frac{\mu}{\bar{u}} \mathbf{T}_{T_2} (\mathbf{U}_m + \mathbf{U}_2),$$

where the upper sign is for the upper surface and the lower sign for the lower surface.

## Acknowledgements

MS and GC acknowledge Region Puglia for having supported the research activity through the constitution of the TRASFORMA Laboratory Network cod. 28. MS also acknowledges the Tribology group for the kind hospitality received during his visit to the Department of Mechanical Engineering of Imperial College London, where part of this work has been performed.

## References

- 1 D. Dowson, 1998. *History of Tribology*. Instn Mech. Engrs, London, UK.
- 2 F. P. Bowden, D. Tabor, 1950. *The friction and lubrication of solids*. Oxford University Press.
- 3 B. N. J. Persson, 2000. *Sliding friction: Physical principles and applications*. Springer.
- 4 M. Scaraggi, 2010. Contact and friction modeling of rough surfaces in dry and lubricated contacts. PhD thesis, Politecnico di Bari.
- 5 J. F. Archard, Elastic deformation and the laws of friction, *Proc. R. Soc. London, Ser. A*, 1957, **243**(1233), 190–205.
- 6 J. A. Greenwood and J. B. P. Williams, Contact of Nominally Flat Surfaces, *Proc. R. Soc. London, Ser. A*, 1966, **295**(1442), 300–319.
- 7 B. N. J. Persson, Theory of rubber friction and contact mechanics, *J. Chem. Phys.*, 2001, **115**(8), 3840–3861.
- 8 B. N. J. Persson, Contact mechanics for randomly rough surfaces, *Surf. Sci. Rep.*, 2006, **61**, 201–227.
- 9 H. Gao, X. Wang, H. Yao, S. Gorb and E. Arzt, Mechanics of hierarchical adhesion structures of geckos, *Mech. Mater.*, 2005, **37** (2–3), 275–285.
- 10 H. Zhang, D. J. Guo and Z. D. Dai, Progress on gecko-inspired micro/nano-adhesion arrays, *Chin. Sci. Bull.*, 2010, **55**(18), 1843–1850.
- 11 E. Stratakis, A. Ranella and C. Fotakis, Biomimetic micro/nanostructured functional surfaces for microfluidic and tissue engineering applications, *Biomicrofluidics*, 2011, **5**, 013411.
- 12 B. N. J. Persson and M. Scaraggi, On the transition from boundary lubrication to hydrodynamic lubrication in soft contacts, *J. Phys.: Condens. Matter*, 2009, **21**(18), 185002.
- 13 B. N. J. Persson, O. Albohr, U. Tartaglino, A. I. Volokitin and E. Tosatti, On the nature of surface roughness with application to contact mechanics, sealing, rubber friction and adhesion, *J. Phys.: Condens. Matter*, 2005, **17**, R1–R62.
- 14 D. Dowson, Modelling of Elastohydrodynamic Lubrication of Real Solids by Real Lubricants, *Meccanica*, 1998, **33**, 47–58.
- 15 H. A. Spikes, Sixty years of EHL, *Lubr. Sci.*, 2006, **18**, 265–291.
- 16 B. N. J. Persson and C. Yang, Theory of the leak-rate of seals, *J. Phys.: Condens. Matter*, 2008, **20**(31), 315011.
- 17 B. Lorenz and B. N. J. Persson, Leak rate of seals: Effective-medium theory and comparison with experiment, *Eur. Phys. J. E*, 2010, **31**(2), 159–167.
- 18 F. Bottiglione, G. Carbone, L. Mangialardi and G. Mantriota, Leakage Mechanism in Flat Seals, *J. Appl. Phys.*, 2009, **106**(10), 104902.
- 19 B. Lorenz and B. N. J. Persson, Leak rate of seals: Comparison of theory with experiment, *Europhys. Lett.*, 2009, **86**, 44006.

- 20 P. Sperka, I. Krupka and M. Hartl, Experimental study of real roughness attenuation in concentrated contacts, *Tribol. Int.*, 2010, **43**, 1893–1901.
- 21 C. J. Hooke and C. H. Venner, Surface roughness attenuation in line and point contacts, *Proc Inst. Mech. Eng., Part J*, 2000, **214**(5), 439–444.
- 22 C. H. Venner and A. A. Lubrecht, An engineering tool for the quantitative prediction of general roughness deformation in EHL contacts based on harmonic waviness attenuation, *Proceedings of the Institution of Mechanical Engineers Part J-Journal of Engineering Tribology*, 2004, **219**(42), 303–312.
- 23 C. J. Hooke and K. Y. Li, Rapid calculation of the pressures and clearances in rough, elastohydrodynamically lubricated contacts under pure rolling. Part 1: low amplitude, sinusoidal roughness, *Proc. Inst. Mech. Eng., Part C*, 2006, **220**(6), 901–913.
- 24 C. J. Hooke and K. Y. Li, Rapid calculation of the pressures and clearances in rough, elastohydrodynamically lubricated contacts under pure rolling. Part 2: general roughness, *Proc. Inst. Mech. Eng., Part C*, 2006, **220**(6), 915–925.
- 25 J. H. H. Bongaerts, K. Fourtouni and J. R. Stokes, Soft-tribology: Lubrication in a compliant PDMS–PDMS contact, *Tribol. Int.*, 2007, **40**, 1531–1542.
- 26 M. Scaraggi, G. Carbone and D. Dini, Experimental Evidence of Micro-EHL Lubrication in Rough Soft Contacts, *Tribol. Lett.*, 2011, **43**(2), 169–174.
- 27 N. Patir and H. S. Cheng, Average flow model for determining effects of 3-dimensional roughness on partial hydrodynamic lubrication, *J. Lubr. Technol.*, 1978, **100**(1), 12–17.
- 28 N. Patir and H. S. Cheng, Application of average flow model to lubrication between rough sliding surfaces, *J. Lubr. Technol.*, 1979, **101**(2), 220–230.
- 29 D. C. Sun, Effects of 2-dimensional Reynolds roughness in hydrodynamic lubrication, *Proc. R. Soc. London, Ser. A*, 1978, **364** (1716), 89–106.
- 30 W. L. Li, Some discussions on the flow factor tensor—considerations of roughness orientation and flow rheology, *J. Tribol.*, 2000, **122**(4), 869–872.
- 31 S. R. Harp and R. F. Salant, An average flow model of rough surface lubrication with inter-asperity cavitation, *J. Tribol.*, 2001, **123**(1), 134–143.
- 32 M. Prat, F. Plouraboué and N. Letalleur, Averaged Reynolds Equation for Flows between Rough Surfaces in Sliding Motion, *Transport in Porous Media*, 2002, **48**, 291–313.
- 33 A. Almqvist and J. Dasht, The homogenization process of the Reynolds equation describing compressible liquid flow, *Tribol. Int.*, 2006, **39**(9), 994–1002.
- 34 F. Sahlin, A. Almqvist, R. Larsson and S. Glavatskih, Rough surface flow factors in full film lubrication based on a homogenization technique, *Tribol. Int.*, 2007, **40**(7), 1025–1034.
- 35 F. M. Meng, S. Q. Cen, Y. Z. Huc and H. Wang, On elastic deformation, inter-asperity cavitation and lubricant thermal effects on flow factors, *Tribol. Int.*, 2009, **42**(2), 260–274.
- 36 M. Scaraggi, G. Carbone and D. Dini, Lubrication in soft rough contacts: A novel homogenized approach. Part II - Discussion, *Soft Matter*, 2011, **7**, DOI: 10.1039/c1sm05129f.
- 37 M. Scaraggi and G. Carbone, Transition from elastohydrodynamic to mixed lubrication in highly loaded squeeze contacts, *J. Mech. Phys. Solids*, 2010, **58**(9), 1361–1373.
- 38 B. N. J. Persson, Contact mechanics for randomly rough surfaces, *Surf. Sci. Rep.*, 2006, **61**(4), 201–227.
- 39 G. Carbone, B. Lorenz, B. N. J. Persson and A. Wohlers, Contact mechanics and rubber friction for randomly rough surfaces with anisotropic statistical properties, *Eur. Phys. J. E*, 2009, **29**(3), 275–284.
- 40 B. N. J. Persson, Relation between Interfacial Separation and Load: A General Theory of Contact Mechanics, *Phys. Rev. Lett.*, 2007, **99** (12), 125502.
- 41 C. Yang and B. N. J. Persson, Contact mechanics: contact area and interfacial separation from small contact to full contact, *J. Phys.: Condens. Matter*, 2008, **20**(21), 215214.
- 42 O. Reynolds, On the Theory of Lubrication and Its Application to Mr. Beauchamp Tower's Experiments, Including an Experimental Determination of the Viscosity of Olive Oil, *Philos. Trans. R. Soc. London*, 1886, **177**, 157–234.
- 43 F. A. Howes and S. Whitaker, The spatial averaging theorem revisited, *Chem. Eng. Sci.*, 1985, **40**(8), 1387–1392.
- 44 K. Tønder, Mathematical verification of the applicability of modified reynolds equations to striated rough surfaces, *Wear*, 1977, **44**, 329–343.
- 45 B. N. J. Persson, Fluid dynamics at the interface between contacting elastic solids with randomly rough surfaces, *J. Phys.: Condens. Matter*, 2010, **22**(26), 265004.
- 46 M. Scaraggi, F. Bottiglione, G. Carbone, 2010. On the fluid dynamics in static sealing. In preparation.
- 47 B. N. J. Persson and F. Mugele, Squeeze-out and wear: fundamental principles and applications, *J. Phys.: Condens. Matter*, 2004, **16**, R295.
- 48 P. Martin and F. Brochard-Wyart, Dewetting at Soft Interfaces, *Phys. Rev. Lett.*, 1998, **80**(15), 3296–3299.
- 49 B. N. J. Persson, A. Volokitin and E. Tosatti, Role of the external pressure on the dewetting of soft interfaces, *Eur. Phys. J. E*, 2003, **11**(4), 409–413.
- 50 D. Stauffer, A. Aharony, 2003. *Introduction to Percolation Theory*. 2nd Revised Edition, Taylor & Francis.